Protein Secondary Structure and Orientation in Silk as Revealed by Raman Spectromicroscopy

Thierry Lefèvre, Marie-Eve Rousseau, and Michel Pézolet
Centre de Recherche en Sciences et Ingénierie des Macromolécules, Centre de Recherche sur la Fonction, la Structure et l'Ingénierie des Protéines, Département de Chimie, Université Laval, Pavillon Alexandre-Vachon, Québec, Canada

ABSTRACT Taking advantage of recent advances in polarized Raman microspectroscopy, and based on a rational decomposition of the amide I band, the conformation and orientation of proteins have been determined for cocoon silks of the silkworms *Bombyx mori* and *Samia cynthia ricini* and dragline silks of the spiders *Nephila clavipes* and *Nephila edulis*. This study distinguished between band components due to β-sheets, β-turns, 3_1-helices, and unordered structure for the four fibers. For *B. mori*, the β-sheet content is 50%, which matches the proportion of residues that form the GAGAGS fibroin motifs. For the *Nephila* dragline and *S. c. ricini* cocoon, the β-sheet content (36–37% and 45%, respectively) is higher than the proportion of residues that belong to polyalanine blocks (18% and 42%, respectively), showing that adjacent GGA motifs are incorporated into the β-sheets. *Nephila* spidroins contain fewer β-sheets and more flexible secondary structures than silkworm fibroins. The amorphous polypeptide chains are preferentially aligned parallel to the fiber direction, although their level of orientation is much lower than that of β-sheets. Overall, the results show that the four silks exhibit a common molecular organization, with mixtures of different amounts of β-sheets and flexible structures, which are organized with specific orientation levels.

INTRODUCTION

Silk is a filament made of fibrous proteins that is solely produced by arthropods, especially insects and arachnids. Several types of silk can be found in nature, each one having a specific function and exhibiting appropriate mechanical properties. Among all the silks, one class includes fibers that have a high tensile strength (typically 1 $GN.m^{-2}$) and a relatively large extensibility (20–35%) compared to other biological materials, such as cellulose or collagen (1). This class is exemplified by the cocoon silk of silkworms and the dragline silk of spiders. It is structurally characterized by the presence of crystallites composed of pleated β-sheets that are preferentially aligned parallel to the fiber axis (1,2). This type of silk is generally viewed as a semicrystalline material in which the crystallites are dispersed in an amorphous matrix and seem to act as reinforcing junction zones (3,4). However, the mechanical properties of silk are actually determined by its hierarchical structural assembly at all length scales. This includes the possible presence of nanoscale features such as nanofibrils (5–9), skin/core organization (10,11), or nanodomains (8,12), the level of crystallinity, the size and distribution of the crystallites, and the conformational and orientational organization at the molecular level.

The molecular arrangement of silk results from the spinning process and the protein primary structure. Silk proteins, the so-called fibroins for silkworms and spidroins for spiders, are composed of repetitive sequences that can be divided into smaller motifs or blocks. Fig. 1 shows typical repeating protein amino acid sequences of the cocoon silk of the domestic silkworm *Bombyx mori* (13,14) and wild silkworm *Samia cynthia ricini* (K. Yukuhiro, National Institute of Agrobiological Sciences, personal communication, 2002), and the dragline silk of the orb-weaving spider *Nephila clavipes* (15,16). For the latter, two spidroins synthesized in the major ampullate glands, MaSp1 and MaSp2, actually make up the dragline thread, MaSp1 being the most abundant (16–18). As a first approximation, the primary structure of silk can be divided into a β-sheet-forming domain and a second segment that constitutes the amorphous phase. Although the amounts of β-sheets have not been determined, a consensus has emerged about the sequences involved in β-sheet crystallites. The GAGAGS motif of *B. mori*'s cocoon silk has been found to form pleated β-sheets (19,20). For the spiders' spidroins, the polyalanine (Ala_n) segments have been identified as the building blocks of the β-sheets (16,21,22). The fibroin of *S. c. ricini* cocoon contains polyalanine runs that are longer than those of the spider dragline and also appear to adopt the β-sheet structure (23,24).

The rest of the protein molecule is assumed to form the amorphous phase of silk and is characterized by several glycine (*N. clavipes*, *S. c. ricini*) or tyrosine (*B. mori*) residues. The secondary structures adopted by this sequence are generally unknown, admitted to be random, or debated. In the case of *B. mori*, this amino acid segment is dominated by the GAGAGY motif and, to a lesser extent, by GAAS and GAGVGAGY blocks (14). It has been proposed that half of this amorphous sequence forms distorted β-turns, the other half adopting distorted β-sheets (25). The tyrosine residues may locally induce randomness in the fibroin backbone (26), whereas it has been suggested that the GAAS motif forms

Submitted November 2, 2006, and accepted for publication December 15, 2006.

Address reprint requests to Michel Pézolet, Département de Chimie, Université Laval, Pavillon Alexandre-Vachon, Québec G1K 7P4, Canada. Tel.: 418-656-2481; Fax: 418-656-7916; E-mail: michel.pezolet@chm.ulaval.ca.

0006-3495/07/04/2885/11 $2.00

doi: 10.1529/biophysj.106.100339

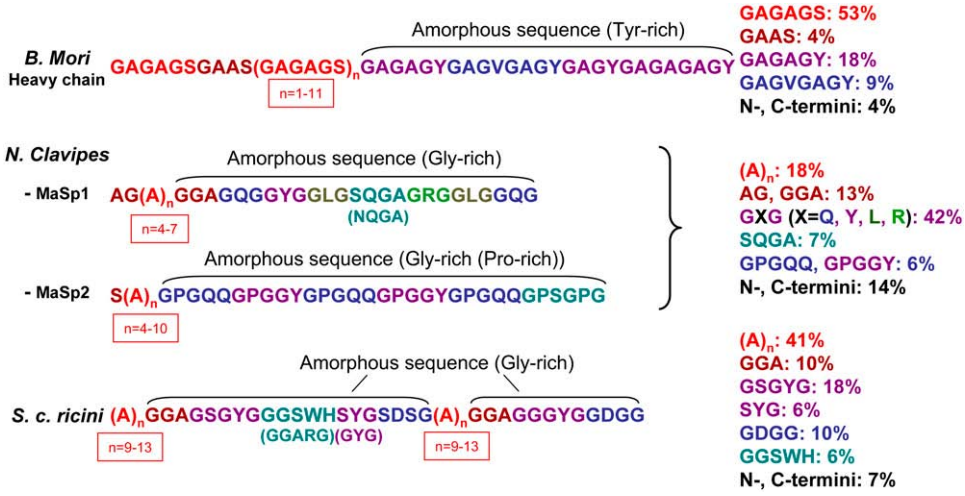

FIGURE 1 Typical repetitive amino acid sequences of silk proteins (based on Mita et al. (13), and Zhou et al. (14) for *B. mori* and on Hinnan and Lewis (16) and Brooks et al. (17) for *N. clavipes*, respectively. The primary structure of *S. c. ricini* is from a personal communication (2002) with K. Yukuhiro, National Institute of Agrobiological Sciences). Amino acids in red indicate sequence motifs that are recognized in the literature as being involved in β-sheets. Other colors differentiate amino acid motifs that are assumed to compose the amorphous regions of silk. Brown amino acids are adjacent to the β-sheet-forming blocks. Motifs between parentheses are frequently encountered amino acid substitutions. The percentages represent the contents of amino acids involved in principal sequence motifs. The compositions of amino acids of dragline silk of *N. clavipes* were calculated using a MaSp1/MaSp2 molar ratio of 9:1 based on our own results obtained by NMR spectroscopy (to be published).

β-turns (27) or β-sheets (26). For the spidroin MaSp1, the glycine-rich sequence is dominated by the tripeptides GGA and GXG (where X = Q, Y, L, or R), whereas the amorphous part of MaSp2 is proline-rich and is dominated by the pentapeptides GPGQQ and GPGGY. The latter have been proposed to form successions of β-turns (β-spirals) that would contribute to the large extensibility of dragline silk (28). It has been proposed that glycine residues may be incorporated into β-sheet crystallites (22,29–36), which may create an interphase between the crystallites and the amorphous matrix that would be important for the mechanical properties of silk. Several studies have also inferred the presence of 3_1-helices in the amorphous region of the dragline fiber (22,33–35,37). The amorphous part of *S. c. ricini*'s fibroin contains GGA motifs like MaSp1, but GGGY (or GSGY), GGSWH (or GGARG), and SDGG (or GDGG) blocks are also present (K. Yukuhiro, National Institute of Agrobiological Sciences, personal communication, 2002). This fiber has been less studied, but based on solid-state ^{15}N and ^{13}C NMR spectroscopy, 65% of the glycine residues would be involved in oriented domains (23).

The determination of the orientation of the polypeptide chains is the second molecular parameter that is required to obtain a complete view of the organization of silk protein molecules. Only scarce data about orientation are available, although the crystallites are acknowledged to be highly oriented. Indeed, x-ray diffraction on *N. clavipes* dragline (38) has shown that the protein chains of the crystalline fraction are oriented along the fiber axis with a Gaussian distribution with a width of 23°. In the amorphous region, the chains are often considered as randomly oriented, but a few studies of the spider dragline suggest that this part of the protein may also be aligned along the fiber axis. ^2H solid-state NMR experiments (29) have shown that the alanine residues of the *N. clavipes* dragline silk are represented by a highly and a weakly oriented population containing 40% and 60% of the alanine residues, respectively. The width of the distribution is 5° for the former and 75° for the latter population. Using wide-angle x-ray diffraction, the molecular chains in the crystals have been described with a Gaussian function (distribution width of 16°) and the amorphous diffraction would be composed of 60% isotropic chains and 40% oriented ones, with a distribution of 30° (31). Finally, from two-dimensional solid-state NMR spectroscopy, the protein backbone revealed a significant level of orientation of both the alanine and glycine residues (34).

The knowledge of the molecular organization is far from being exhaustive, especially because of the scarcity of methods with the capacity to provide quantitative data relative to the overall protein secondary structures and their orientation. Two major advances accomplished recently in Raman spectromicroscopy can help to overcome this limitation. First, a method has been developed to determine the order parameters P_2 and P_4 of the orientation function of protein carbonyl groups (39). Second, to determine the secondary structures in oriented protein samples, a procedure has been proposed to calculate an orientation-insensitive spectrum, i.e., a spectrum that is only representative of the molecular conformation, without contributions from the orientation of the molecules (40). One remarkable advantage of Raman spectromicroscopy is that the measurements can be performed on a single filament. Therefore, based on state-of-the-art Raman instrumentation and analysis, and using a rational spectral decomposition procedure on the amide I band, this study is devoted to 1), defining the protein conformation, taking into account the diversity and proportions

of the secondary structures present; and 2), determining the orientation level of the polypeptide chains in the β-sheets and in the amorphous phase, and then estimating the distribution of orientation. This quantification of the secondary structures and orientation has been carried out on the cocoon silk of *B. mori* and *S. c. ricini* silkworms and on the dragline silks of two spiders of the genus *Nephila*, i.e., *N. clavipes* and *Nephila edulis*.

EXPERIMENTAL

Materials

Cocoon fibers from the silkworm *B. mori* were supplied by the Insects Production Unit of the Canadian Forest Service (Sault Ste. Marie, Ontario, Canada). Raw silk of *B. mori* cocoons was degummed in boiling water containing sodium bicarbonate (0.05% w/v) for 15 min. The resulting material was rinsed thoroughly with deionized water and dried under vacuum. *S. c. ricini* fibers were a gift from Dr. Tetsuo Asakura (Department of Biotechnology, Tokyo University of Agriculture and Technology, Tokyo, Japan). To remove the sericin coating, *S. c. ricini* cocoons were degummed three times with a sodium peroxide solution (0.1% w/v) alternating with rinsing with boiling distilled water. Dragline silk fibers from the spider *N. clavipes* came from adult female spiders collected in Florida. The dragline was reeled from awake spiders at 0.5 $cm.s^{-1}$. *N. edulis* dragline silk fibers were a gift from Prof. Marie E. Herberstein (Department of Biological Sciences, Macquarie University, Sydney, Australia) and Prof. Frances Separovic (Department of Chemistry, Melbourne University, Melbourne, Australia). The samples came from adult female spiders collected from Queensland, in Australia, and the dragline was reeled from awake spiders. They were rinsed with acetone before shipment, and, upon reception, were kept in a dry environment at 4°C, hidden from sunlight to avoid degradation. The spectra were recorded more than one month after silk spinning.

Regenerated films made from cocoon silk fibroins were also prepared. For *B. mori*, degummed cocoon fibers were solubilized with 9 M LiBr at 40°C for 20 min. The salt was removed by dialyzing the solution against deionized water using cellulose tubing (12- to 14-kDa cut-off). The dialyzed solutions were cast onto polyethylene films and dried for 48 h in dry air, which resulted in films with a thickness of ~25 μm. For *S. c. ricini*, the dope solution was collected directly from the gland, diluted in water, and allowed to dry. The resulting regenerated films from cocoon silks were immersed in a 50% v/v methanol aqueous solution to induce the formation of β-sheets in the samples, and then air-dried.

Methods

For Raman measurements, films and silk monofilaments were gently mounted on glass microscope slides with double-sided tape. Spectra were recorded at 22 ± 0.5°C at a relative humidity of 20 ± 5% using a LABRAM 800HR Raman spectrometer (Horiba Jobin Yvon, Villeneuve d'Ascq, France) coupled to an Olympus BX 30 fixed-stage microscope. The 514.5-nm line of an Ar^+ laser (INNOVA 70C Series Ion Laser, Coherent, Santa Clara, CA) was chosen for *B. mori* and *N. clavipes* samples, whereas the 632.8-nm line of a He-Ne laser (Melles Griot, Carlsbad, CA) was used for the *N. edulis* and *S. c. ricini* fibers. The laser beam was focused with a 100× objective (0.9 NA, Olympus, Melville, NY) to a diameter of ~1 μm, generating an intensity at the sample of ~5 mW (green line) and 7 mW (red line). The confocal hole and the entrance slit of the monochromator were fixed at 200 and 100 μm, respectively. Data were collected by a 1-inch open-electrode Peltier-cooled CCD detector (1024 × 256 pixels). A half-wave plate (Melles Griot) was used to rotate the polarization of the incident laser beam. A polarizer was placed before the entrance slit of the monochromator to allow the detection of the polarized scattered light. A broadband quarter-wave plate was placed after the polarizer to eliminate the polarization dependence of the grating. The measurement time of a single spectrum was typically ~1 min. No sign of sample deterioration was observed under these experimental conditions. The spectra were corrected to account for the polarization dependence of the instrument using isotropic samples such as films of globular or silk proteins (39).

Data analysis

All spectral manipulations were performed using GRAMS/AI 7.0 (ThermoGalactic, Salem, NH). The spectra were first corrected for a small fluorescence background over the 600–1800 cm^{-1} spectral range using a polynomial baseline. Then they were 5–9 points smoothed and a linear baseline was subtracted in the amide I region (1750–1570 cm^{-1}). Spectra obtained from different experiments were corrected for a small wavenumber shift using the tyrosine band at 1615 cm^{-1}. Nine spectra were recorded at three different points on three different samples. The mean spectrum was then calculated and used for the spectral analysis.

Orientation

For systems showing uniaxial symmetry, the order parameters P_2 and P_4, the first two coefficients of the expansion in Legendre polynomials of the orientation distribution function, can be calculated by Raman spectromicroscopy (39,41,42). The method used is applicable to vibrational mode for which the Raman tensor is cylindrical. However, recent investigations of the amide I mode of crystals of hydrated glycylglycine (43) and of aspartame (44) have shown that the tensor of the amide I vibration is not cylindrical. For adequately chosen axes of reference, the Raman tensor $\overline{\overline{\alpha}}$ can be written

$$\overline{\overline{\alpha}} = \begin{pmatrix} \alpha_1 & & \\ & \alpha_2 & \\ & & \alpha_3 \end{pmatrix} = \alpha_3 \begin{pmatrix} \alpha_1/\alpha_3 & & \\ & \alpha_2/\alpha_3 & \\ & & 1 \end{pmatrix} (\alpha_1 = \alpha_2 \text{ for a cylindrical tensor}).$$

The results of both studies show that α_3 is much larger than α_1 and α_2, but the values of the tensor elements significantly differ (Table 1). To determine the effect of the shape of the Raman tensor, we have made orientation calculations for the amide I band of *N. clavipes*'s dragline silk using both published Raman tensors and a cylindrical Raman tensor. In the latter case, the parameter $a = \alpha_1/\alpha_3 = \alpha_2/\alpha_3$ was determined from the experimental depolarization ratio R_{iso} as measured from an isotropic sample. To this end, we have used β-sheet-rich regenerated films made from the cocoon silks of *B. mori* and *S. c. ricini*. As shown in Table 1, all three Raman tensors give, within experiment errors, the same value for the order parameter P_2, and thus the same level of orientation. We believe that this result is due to the fact that for the amide I mode, the α_3 element is much bigger than the α_1 and α_2

TABLE 1 Ratios of the elements of the amide I Raman tensors and corresponding order parameters P_2 and P_4 calculated for the *N. edulis* dragline

	α_1/α_3	α_2/α_3	P_2	P_4
Pajcini et al. (43)	0.274	−0.016	−0.34 ± 0.02	0.21 ± 0.02
Tsuboi et al. (44)	0.200	0.050	−0.32 ± 0.02	0.19 ± 0.02
Cylindrical Raman tensor	0.164	0.164	−0.31 ± 0.02	0.12 ± 0.02

P_2 and P_4 were determined from the experimental amide I intensity ratios $R_1 = 0.31$ and $R_2 = 0.11$.

elements, so that it dominates the orientation results. On the other hand, the value of P_4, which essentially determines the shape of the orientation distribution, is smaller for the cylindrical tensor compared to those obtained for noncylindrical Raman tensors. The most probable distributions of orientation calculated by the three tensors all have a maximum at 90°, but the distributions calculated from the results of Pajcini and co-workers (43) and Tsuboi and co-workers (44) are slightly narrower than the one calculated from a cylindrical Raman tensor (data not shown). However, the results of those studies (43,44) lead to a distribution of orientation that is slightly bimodal, whereas the distribution is more Gaussian for a cylindrical Raman tensor. Since there is no compelling argument to favor the Raman tensor of Pajcini et al. (43) at the expense of that of Tsuboi et al. (44), and since the orientation results are basically unaffected by the differences between the three tensors, we have decided to use the values of the order parameters obtained for a cylindrical Raman tensor, as done in previous studies (39,45).

The calculation procedure is based on the measurement of four polarized spectra by Raman spectromicroscopy in the backscattering configuration (39,41,42). From these spectra, two intensity ratios for a given band $R_1 = I^{\mu}_{ZX}/I^{\mu}_{ZZ}$ and $R_2 = I^{\mu}_{XZ}/I^{\mu}_{XX}$ can be calculated, where I^{μ}_{ij} ($i, j = x, z$) are the polarized Raman intensities when the incident laser beam is polarized along the i axis and the scattered Raman radiation is polarized along the j axis. The coordinate system (x, y, z) defines the laboratory frame, the z axis, corresponding to the fiber long axis, and the y axis, corresponding to the propagation direction of the incident and scattered light (39). The order parameters P_2 and P_4 can be calculated from the ratios R_1 and R_2, and from the parameter a. Finally, from P_2 and P_4, the most probable orientation distribution $N_{mp}(\theta)$ of the considered chemical group can be estimated using the information theory (θ is the angle around the fiber axis) (46,47). It has been shown that the z axis of the amide I Raman tensor is oriented at 33° from the carbonyl group of peptide bonds (43,44). The orientation of the amide I Raman tensor is thus close but different from the orientation of the carbonyl group.

Orientation-insensitive spectrum

A spectrum of a uniaxially oriented sample free from spectral contributions due to orientation and only sensitive to molecular conformation can be calculated from a linear combination of polarized spectra obtained by conventional Raman spectroscopy. The orientation-insensitive intensity I^{iso} at a Raman shift $\bar{\nu}$ is given by (48)

$$I^{iso}(3 + 6R_{iso}) = I_{zz} + 2I_{xx} + 4I_{xz} + 2I_{xy},$$

where I_{XX}, I_{XZ}, I_{XY}, and I_{ZZ} are the polarized intensities as measured by conventional Raman spectroscopy. For Raman spectromicroscopy, the calculation of I^{iso} is more complex but can nevertheless be carried out from the four intensities I^{μ}_{XX}, I^{μ}_{XZ}, I^{μ}_{ZX}, and I^{μ}_{ZZ} (40).

Curve fitting

Spectral decompositions of the spectra of the amide I band have been carried out using a rational procedure that has been successfully applied to regenerated *S. c. ricini* silk fibroin (45). The choice of the number of components of the amide I band is based on the following criteria in order of increasing importance: 1), the minimum number of components; 2), acknowledged secondary structures present in the system; 3), spectral criteria (second derivatives, deconvolutions, and/or difference spectra); and 4), generation of a reasonable fit (may require additional bands).

In the case described here, apart from the β-sheets that are well recognized to be present in silk fibers, no definite information was available about other secondary structures. A preliminary investigation for *S. c. ricini* fibroin (not shown) using the experimental polarized spectra, second derivatives, and difference spectra has clearly revealed the presence of five amide I components located typically at 1640, 1656, 1667, 1680, and 1695 cm^{-1}, the exact band position and intensity depending on the type of silk (45). Finally, two bands at 1597 and 1615 cm^{-1} are associated with tyrosine side-chain vibrations.

Spectra have been decomposed with mixtures of Lorentzian and Gaussian functions. However, it is known that, from the point of view of physics, Raman bands should have a Voigtian profile. Therefore, some spectral decomposition tests have also been carried out using Voigt functions. The results obtained show clearly that any Voigtian profile can be fitted with a combination of Lorentzian and Gaussian functions. Therefore, since in our case the aim of the spectral decomposition is not to retrieve the real vibrational bandshape (by taking into account the convolution due to the spectrometer or molecular interactions), there is no particular advantage in using Voigtian bands. In addition, the use of mixtures of Lorentzian and Gaussian functions allows independent control of the shape and width of a band during the curve-fitting. On the contrary, changing the Gaussian halfwidth (or the Lorentzian halfwidth) of a Voigtian profile results in modifications of both the total halfwidth and the shape of the band, which prevents a correct independent control of these two parameters. Since our tests show that there is neither real advantage for the analysis of our results nor improvement of the results by the use of Voigtian profiles, it appears that it is legitimate to make spectral decompositions using mixtures of Lorentzian and Gaussian functions. This is indeed a common practice in the literature. The percentage of the Lorentzian character of a band is called %L.

The spectral curve-fitting procedure can be summarized as follows. The method is based on the decomposition of the four polarized spectra of a given sample. It is assumed that the amide I band of the polarized spectra can be resolved into the same set of components (same positions, bandwidth, and %L), the contribution of each component depending on the polarization configuration. Therefore, only variations in intensity between the different polarized spectra are allowed for a given component. In practice, however, small and controlled differences in the position, bandwidth, and %L of a given component are tolerated. Finally, the orientation-insensitive spectrum has been curve-fitted with the initial parameters that have been found to be successful to decompose the corresponding polarized spectra. In general, the maximum variation on the frequency of a given component is ± 0.5 cm^{-1} between the different spectra of a given silk. The maximum variation on the bandwidth is ± 1 cm^{-1}, whereas the maximum variation of %L is $\pm 10\%$. The depolarization ratio of each component has been evaluated using the above spectral decomposition method that has been applied on the polarized spectra of the β-sheet-rich regenerated isotropic film samples of *B. mori* and *S. c. ricini*. To this end, the initial parameters used for the decomposition of the polarized spectra of the fiber of the same species were directly used to decompose the polarized spectra of the isotropic film. The area of each component divided by the sum of the area of all amide I components was used for the determination of the secondary structure content, assuming that the Raman scattering cross section is the same for all structures.

RESULTS AND DISCUSSION

Structural composition of the silks

Fig. 2 shows the orientation-insensitive spectra of two cocoon (*B. mori* and *S. c. ricini*) and two dragline (*N. clavipes* and *N. edulis*) silk monofilaments in the amide I region. The four amide I bands exhibit a similar shape resembling a reversed funnel, suggesting a common structural pattern. These amide I bands are typical of systems that contain a large number of β-sheets with spectral contributions arising from other secondary-structure elements. Although the spectra have similar characteristic profiles, some differences can also be noticed, showing that the fibers are not identical at the molecular level. For example, the peak maximum at 1665 cm^{-1} for *B. mori* is in agreement with the presence of

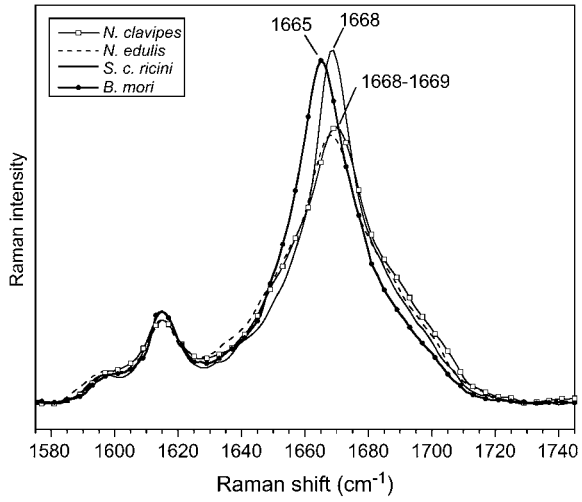

FIGURE 2 Orientation-insensitive Raman spectra of four silk monofilaments in the amide I region. Spectra are normalized with respect to the peak maximum of the amide I band.

antiparallel pleated β-sheets formed by the GAGAGS motif, since the amide I mode of β-poly(L-alanylglycine) ($(AG)_n$) has been found at $\sim$1665 cm^{-1} by normal-mode calculation (49). In the case of *S. c. ricini*, *N. clavipes*, and *N. edulis*, the peak maximum is located at 1668–1670 cm^{-1}, which indicates that the Ala_n blocks are involved in antiparallel pleated β-sheets. Indeed, normal-mode analysis of β-poly (L-alanine) reveals an amide I band at 1669 cm^{-1} (49,50). As mentioned above, apart from the β-sheet component, the amide I band is actually composed of other components representative of the different secondary structures that compose the fiber. As a matter of fact, the amide I bands of *Nephila* dragline fibers are broader than those of the silkworm cocoon fibers, suggesting that the contribution of these structures is more important for the dragline fibers.

To determine the conformation of the silk proteins, the amide I bands were decomposed using the procedure described in the Experimental section. The application of this rational method to the four silks reveals that the amide I band is composed of five components located typically near 1640, 1656, 1667, 1680, and 1695 cm^{-1} (numbered from 1 to 5, respectively), the intensity of each component depending on the type of silk. A similar set of spectral components has already been successfully used to characterize the α-helix-to-β-sheet transition induced by a mechanical stretching of fibroin fibers of *S. c. ricini* fibroins (45). That system was found particularly valuable to test the curve-fitting procedure, since the studied samples contained varying secondary-structure contents (45). That work and this one establish the accuracy of the method and its validity for different silk fibers. The position, bandwidth, and %L of the individual components resulting from this spectral decomposition are given in Table 2. A typical example of spectral decomposition is presented in Fig. 3 for the dragline silk fiber of *N. edulis*.

TABLE 2 Band parameters of the amide I components of the orientation-insensitive spectra for four silk fibers

	Component	1	2	3	4	5
	Assignment	Unordered	3_1-helix	β-sheet	β-turn	β-turn
N. clavipes	Position/cm^{-1}	1641	1656	1670	1685	1700
	FWHH/cm^{-1}	22	17	16	20	20
	%L	47	7	8	20	55
N. edulis	Position/cm^{-1}	1639	1656	1669	1684	1698
	FWHH/cm^{-1}	22	19	16	18	20
	%L	8	19	14	25	38
S. c. ricini	Position/cm^{-1}	1643	1657	1669	1682	1697
	FWHH/cm^{-1}	22	14	13	19	20
	%L	15	48	41	28	29
B. mori	Position/cm^{-1}	1639	1655	1666	1678	1693
	FWHH/cm^{-1}	22	17	16	18	20
	%L	43	4	42	25	0

The fact that the four fibers under study can be decomposed by closely related sets of band components (i.e., by the same model) suggests that the types of secondary structure adopted by the proteins are basically the same, which confirms the occurrence of a common structural molecular pattern. For a given component, some variations in the position, bandwidth, and %L between the different silk samples suggest minor differences in the secondary structure. These structural distortions most likely result from the disparity in the sequences, since different amino acids cannot adopt identical dihedral angles. Some differences in the arrangement, packing, and interactions between side chains may also affect the position of the Raman bands.

As discussed above, component 3 is assigned to the β-sheet conformation. As can be seen in Table 2, this component is narrower for the *S. c. ricini* sample than for *Nephila* spider silks, showing that the β-sheets are structurally more homogeneous for the former. This is most likely due to the longer Ala_n blocks of *S. c. ricini*, which may promote a better packing of the polypeptide chains. The β-sheet component is also broader for *B. mori*, suggesting a

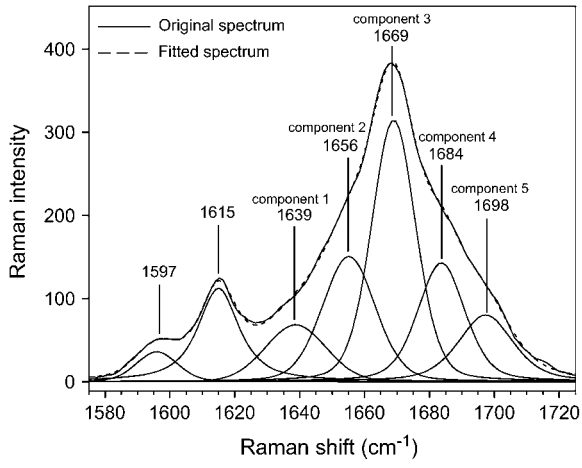

FIGURE 3 Spectral decomposition of the orientation-insensitive spectrum of the dragline silk monofilament of *N. edulis* in the amide I region.

broadly distributed arrangement of the β-sheets. This conclusion is in agreement with x-ray (51) and NMR (25,52) studies showing that the crystalline regions of *B. mori* silk are composed of an irregular stacking of antipolar-antiparallel β-sheet structures in which the alanine residues alternately point to opposite sides of the sheet.

Component 2, at ~1657 cm^{-1}, could be due either to α-helix or 3_1-helix structure, such as polyglycine II (PGII), since normal-mode calculations predict α-helix at 1655 cm^{-1} (α-poly(L-alanine)) and PGII helix at 1654 cm^{-1} (polyglycine) (50). Since no trace of α-helix has been detected experimentally in fibers from *N. clavipes* (21), *Nephila madagascariensis* (22), and *S. c. ricini* by NMR spectroscopy (45), component 2 can confidently be assigned to a PGII or PGII-like conformation. Therefore, from the literature and the data presented here, a consensus seems to emerge about the fact that some threefold helices are present in silk fibers. Eles and Michal have also proposed a PGII structure for *N. clavipes* dragline fiber (35), but they stress that a more complete model should consider other secondary structures as well. The Raman results presented in this article further emphasize the presence of other spectral secondary structures.

The assignment of components 1, 4, and 5 of the four silk samples is not straightforward. Component 1 is likely to arise from unordered (random) structures (53,54). From normal-mode analysis of polypeptides, the position of the amide I band of β-turns has been found to arise over a wide range of wavenumbers, especially in the high-frequency region of the amide I band (55). Considering a transition dipole coupling, $\Delta\mu_{eff}$ (effective dipole moment), between 0.35 and 0.45 D for the amide I mode of turns (56), two main amide I wavenumber domains due to peptide bonds in type I and type III β-turns were found at 1690–1702 cm^{-1} and 1679–1686 cm^{-1}. These spectral regions correspond remarkably well to the components appearing near 1695 and 1680 cm^{-1}, respectively. Therefore, the two former bands are assigned to turns, most probably to type I and type III β-turns, as the wavenumbers of type II β-turns do not match the position of the observed components very well (56). Furthermore, the relatively large bandwidths of components 4 and 5 (18–20 cm^{-1}) suggest that turns may be distorted (55) and/or that other minor secondary structures can contribute.

Finally, taken together, our results suggest that the four silk fibers studied are composed of the same secondary structure elements (essentially β-sheets, turns, 3_1-helix, and random structures), although the content of each secondary structure is specific to each type of silk (see below).

CONFORMATION

The spectra of Fig. 2 can be used to evaluate the amount of secondary structures for the different silks. Based on the above spectral curve-fittings, the areas of each component normalized with respect to the whole amide I band have been calculated and are presented in Fig. 4. The inset table contains

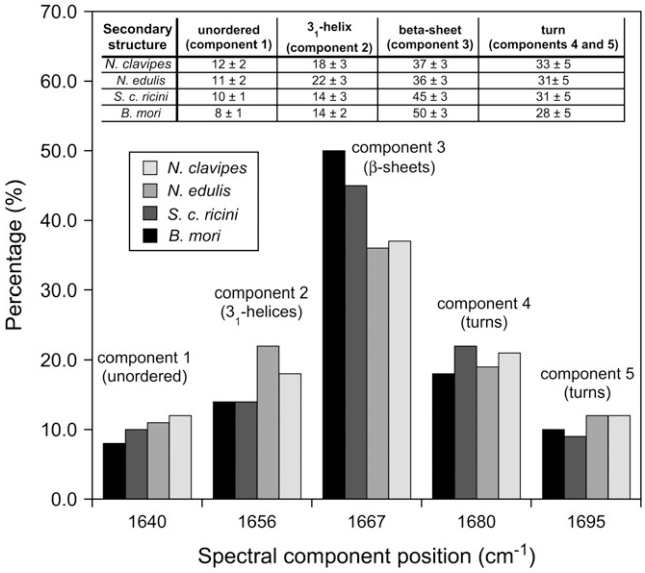

FIGURE 4 Band areas of the different amide I components normalized with respect to the total area of the amide I band (sum of the areas of all amide I components). The inserted table gives the percentages of the different secondary structures. The contents of turns were calculated from the sum of components 4 and 5.

the percentages of secondary structures with the estimated uncertainty. It can be seen that, for a given component, the area is very close for the two dragline silks. Table 2 also shows a very close similarity in the position, bandwidth, and shape (%L) of the amide I components for the two spider silks. These results emphasize the fact that there is a remarkable similarity in the conformations of *Nephila* dragline spidroins. The cocoon silks of *S. c. ricini* and *B. mori* also exhibit close secondary structure contents.

As can be seen, the β-sheet component is the most intense for all silks. The amount of β-sheets can interestingly be compared with the proportions of amino acids that belong to sequence motifs recognized as being involved in β-sheets (Fig. 1). In the case of *Nephila* draglines (the primary structure of *N. edulis* is not known but is expected to be close to that of *N. clavipes* (57)), the amino acids that belong to Ala_n blocks represent 18% of the total, which is significantly lower than the β-sheet content. Taking into account the amino acids in the AG and GGA motifs adjacent to the Ala_n runs (Fig. 1), one obtains 31% of all amino acids. This value is close to the 36–37% of β-sheets found for *Nephila* dragline silk and thus strongly suggests that the AG and GGA sequence motifs are included in the β-sheets. This result is in agreement with other reports (22,29–36) that propose the incorporation of glycine residues within the β-sheets. In the case of *S. c. ricini*, the β-sheet content (45%) is also higher than the proportion of amino acid residues of Ala_n sequences (41%). Therefore, other amino acids are most likely involved in β-sheets for *S. c. ricini*. The adjacent GGA motifs represent 10% of the fibroin which, with Ala_n blocks, would lead to 51% of all amino acids, a higher value than the

β-sheet content determined by Raman spectroscopy. Therefore, Raman data suggest that some GGA segments or some residues of the GGA segments would be involved in β-sheets, as they are in *Nephila* draglines. It is probable that the more homogeneous β-sheets formed by *S. c. ricini* fibroin are less favorable to the incorporation of adjacent amino acids. In the case of *B. mori*, the β-sheet content (50%) is close to the proportion of GAGAGS amino acids (53%).

Fig. 4, shows that *Nephila* dragline silks contain significantly fewer β-sheets (36–37%) than silkworm cocoon silks (45–50%). Since the crystallites are formed by β-sheets, a comparison with the crystallinity is relevant. The degree of crystallinity of *Nephila* dragline threads has been found to vary from 11% to 30% (3,38,58,59). These values are lower than those reported for *B. mori* silk, which range from 40% to 55% (60–62). Although there is a fairly broad range of variability about the degree of crystallinity of silk, the lower β-sheet content of the dragline fiber can be coarsely related to its lower crystallinity. In addition, since the number of β-sheets is higher than crystallinity value for the four silks, it is probable that a fraction of the β-sheets is located in the amorphous phase.

The lower contribution of the β-sheet component for the dragline fibers is counterbalanced by ~10–15% more structures, such as turns, 3_1-helices, and random conformations, than the silkworm fibers. These structures are more flexible than the β-sheet and are likely to play an important role in the higher extensibility of the dragline, which is higher than that of the cocoon silk. Among the 42% of the tripeptides GXG (X = Q, Y, L, or R) of the protein sequence of spider's dragline, a large part is likely to be involved in turns since this structure represents 31–33% of the secondary structures, as determined by Raman spectromicroscopy. The GPGXX sequence (5% of the amino acid sequence) is also predicted to adopt turn structures (28,63). Similarly, in the case of *S. c. ricini*, comparison between the number of turns (31%) and the 40% of glycine-containing sequence motifs (GSGY, SGY, GDGG, and GGSWH) leads us to infer that at least some of these amino acid segments also adopt turn conformations.

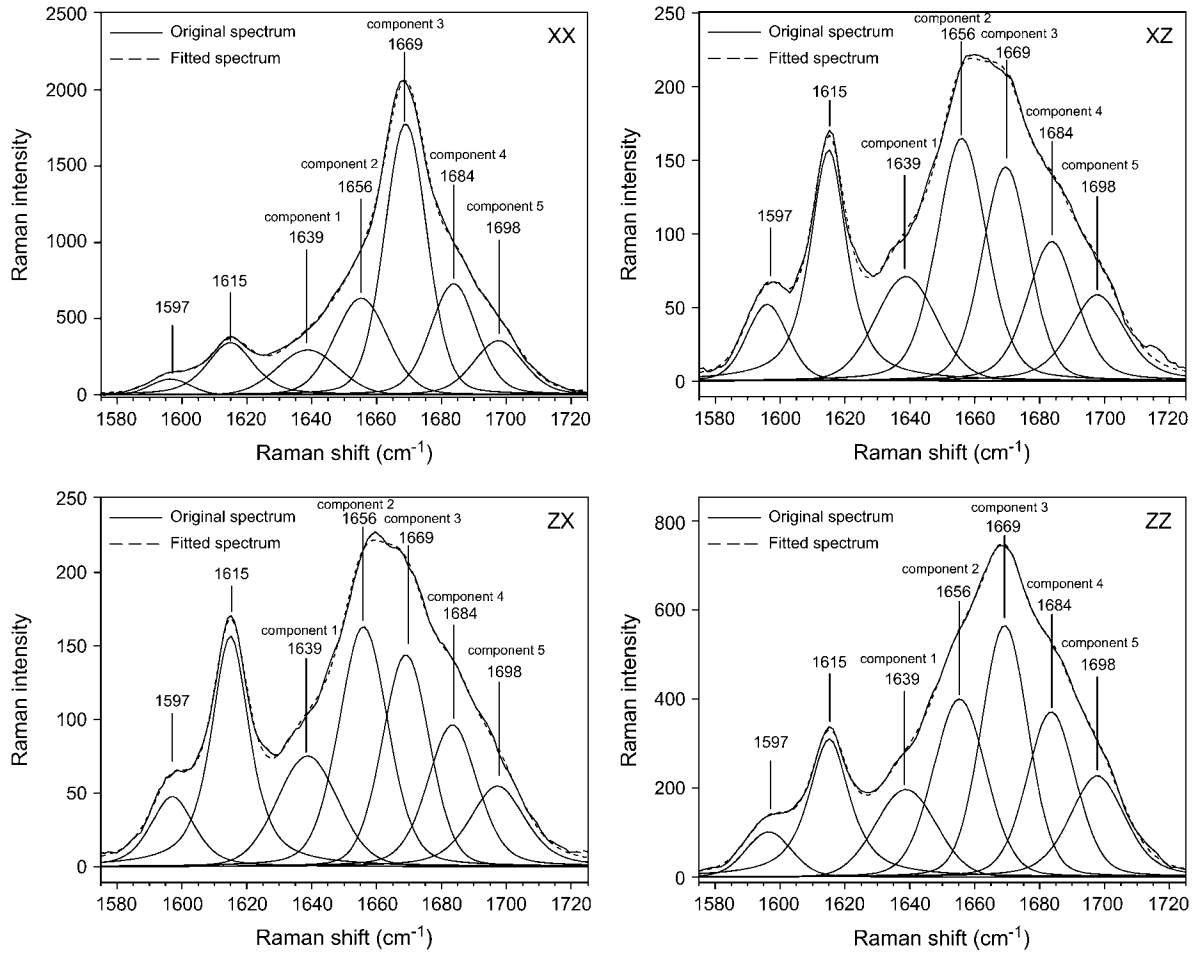

FIGURE 5 Original polarized spectra in the amide I region of the dragline silk monofilament of *N. edulis* in the amide I region and the corresponding spectral decompositions.

Orientation

In conjunction with the protein conformation, the level of molecular orientation is also responsible for the mechanical properties of silk (64). In a previous work (39), the orientation of the β-sheets has been calculated on different silks based on the peak height of the original amide I band, since this secondary structure dominates the spectra. More accurate data about the orientation of the β-sheets can now be obtained by using the spectral components of the amide I band. More importantly, the orientation of polypeptide chain segments that are involved in other secondary structures (i.e., in the amorphous phase) can now be evaluated.

Fig. 5 shows a typical example of the decomposition of the polarized Raman spectra of a silk fiber for the dragline thread of *N. edulis*. As can be noted, the intensity of the xx spectrum is ~3 times higher than that found for the zz polarization. Since the spectrum is dominated by the contribution of the β-sheets, the peak height of the polarized amide I band directly indicates that the amide I tensor is highly oriented perpendicular to the fiber direction (we recall that, in the case of β-sheets, the carbonyl groups are perpendicular to the strand direction). Interestingly, the shape of the polarized spectra, especially the xz and zx ones, nicely reveal shoulders that give evidence of the presence of the different bands used for the decomposition. It can also be noticed that the polarized spectra can be decomposed with the same set of components, which also supports the validity of the spectral decomposition.

A more precise quantitative estimation of the degree of orientation can be obtained from the order parameter P_2, calculated from the intensities of the band components. The theoretical boundary values of P_2 are $+1$ and -0.5, if the Raman tensor of the considered vibrational mode is perfectly oriented parallel and perpendicular to the fiber axis, respectively. Fig. 6 shows the comparison between P_2 values for the four silk samples studied, as calculated from the polarized intensities of the different components. Component 3 displays very negative P_2 values (from -0.37 to -0.45, depending on the type of silk), which indicates a high orientation of the β-sheets along the fiber axis. The P_2 values, however, are more negative than those found previously using the intensity of the entire amide I band (39). This is most likely due to the fact that the peak height of the whole band was first used to calculate the P_2 of the β-sheets with contributions from other secondary structures. Thanks to the spectral decomposition, the intensity of the β-sheet component is free from interference arising from the less oriented secondary structures. For all other components and for the four silks, Fig. 6 reveals unambiguously that all P_2 value are negative, P_2 ranging from -0.06 to -0.23, depending on the component and type of silk. Thus, the protein backbone in the amorphous regions of these silks is not randomly oriented but exhibits a significant level of orientation, although it is much less than that of the β-sheets. This

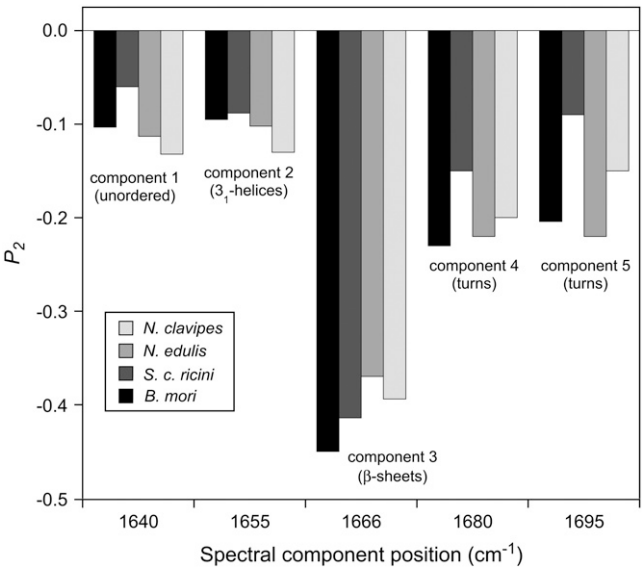

FIGURE 6 Comparison of the order parameter P_2 values of the amide I components for the different silk fibers.

study of the molecular orientation confirms that there exists a structural molecular pattern for the four silks, the β-sheets being highly oriented, the polypeptide chains in the amorphous matrix being partially extended along the fiber axis.

Table 3 presents the order parameters P_2 and P_4, calculated from the intensity of the band components of the four silks. As in the case of the secondary-structure contents, the order parameters of each component are very close for the two *Nephila* spiders, which underlines the strong similarity in the molecular organization of both silks. Based on the P_2 values, it appears that the β-sheets are slightly more oriented for the cocoon fiber than for the dragline, thus confirming our previous results (39). Conversely, the P_2 values of other components are slightly more negative for the spiders than for the silkworms, suggesting a slightly higher level of orientation of the amorphous phase for the spiders.

TABLE 3 Order parameters P_2 and P_4 of the amide I components of the polarized spectra for four silk fibers

	Component	1	2	3	4	5
	assignment	Unordered	3_1-helix	β-sheet	β-turn	β-turn
N. clavipes	P_2 ($\pm$0.02)	−0.13	−0.13	−0.39	−0.2	−0.15
	P_4 ($\pm$0.02)	0.00	−0.03	0.19	0.02	0.00
N. edulis	P_2 ($\pm$0.02)	−0.11	−0.10	−0.37	−0.22	−0.22
	P_4 ($\pm$0.02)	−0.06	−0.08	0.20	0.02	0.02
S. c. ricini	P_2 ($\pm$0.02)	−0.06	−0.10	−0.41	−0.15	−0.09
	P_4 ($\pm$0.02)	−0.13	−0.22	0.24	0.06	0.03
B. mori	P_2 ($\pm$0.02)	−0.10	−0.10	−0.45	−0.23	−0.20
	P_4 ($\pm$0.02)	0.04	−0.20	0.30	0.16	0.12
Isotropic films	R^*_{iso}($\pm$0.02)	0.26	0.27	0.20	0.18	0.18

*The R_{iso} parameter values are averaged from spectral decompositions of the amide I band (not shown) of the β-sheet-rich regenerated films made from *B. mori* and *S. c. ricini* fibroins.

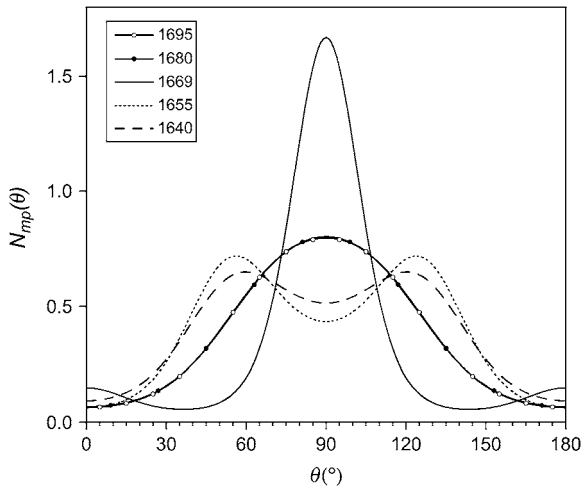

FIGURE 7 Most probable orientation distribution functions of the different amide I components of *N. edulis* dragline silk fiber.

Fig. 7 shows the most probable orientation distribution functions of all amide I components of *N. edulis* dragline, as determined from P_2 and P_4 using information theory. The distribution of orientation of the β-sheets is almost Gaussian with a width of 30° (identical value for *N. clavipes*). This value is higher than that determined by x-ray diffraction (width of 23°) (38), the discrepancy being due to the fact that Raman spectroscopy is sensitive to both crystalline and amorphous domains. The distributions of orientation of components 4 and 5 are also nearly Gaussian, whereas those of components 1 and 2 exhibit a slightly bimodal distribution. In any case, these distributions are much broader than for the β-sheets.

The low degree of molecular orientation within the amorphous phase of natural silks (Table 3 and Fig. 6) means that the chains are not completely extended. This is certainly a parameter that plays a major role in the large extensibility of silk materials by allowing a further alignment of the molecules without rupture upon drawing the native fiber. In addition, for *Nephila* draglines, the presence of large amounts of flexible secondary structures such as turns, 3_1-helices, and random conformations (Fig. 4) seem to provide an additional possible reason for the extension of the silk threads. Thus, both the molecular orientation and the amount of extensible secondary structures contribute to the extensibility of silk. In the case of cocoon silk, the low amount of flexible structures, as found by Raman spectromicroscopy, is likely to limit its extensibility. Finally, the low orientation level of the protein backbone in the amorphous matrix may also contribute to the supercontraction of dragline silk (64). This phenomenon involves a shrinkage along the fiber, accompanied by an increase in its diameter in the presence of water (36,64). The existing orientational order of the amorphous phase and β-sheets in the natural fiber is likely to disappear at least partially upon wetting due to plasticization by water, leading to the contraction of the fiber.

CONCLUSIONS

For the first time, the contents and orientation levels of the secondary structures present in silk monofilaments of cocoon and dragline silks have been determined. The four silk fibers studied exhibit a common structural pattern characterized by mixtures in different amounts of crystallites, amorphous β-sheets, and other more flexible structures, such as β-turns, 3_1-helices, and random structures that are organized with specific levels of orientation. The proportion of each secondary structure varies from one silk fiber to another. The numbers of β-sheets found by Raman spectroscopy closely match the contents of GAGAGS amino acids of *B. mori*. In the case of *Nephila* spiders and *S. c. ricini* silkworm, the β-sheet content is higher than the number of amino acids that belong to Ala_n runs, which suggests that adjacent GGA sequence motifs are incorporated into the β-sheets. The number of β-sheets is higher than the degree of crystallinity, suggesting that some of the β-sheets are located in the amorphous regions. The order parameters P_2 and P_4, as well as the most probable orientation function of each secondary structure, show that the β-sheets are highly oriented along the fiber axis and that the amorphous phase is also oriented, but to a lower extent than for β-sheets. The β-sheets of cocoon silks are slightly more oriented than those of dragline silks, whereas the amorphous chains are slightly more oriented for the dragline silk. Overall, Raman spectromicroscopy data suggest that the high extensibility of spider dragline silk is mainly due to the fact that the polypeptide chains are not completely extended in the amorphous matrix, combined with a high content of extensible structures. The high proportion of β-sheets in cocoon fiber may limit the extensibility of this kind of silk. It would be desirable to extend the knowledge of quantitative parameters that characterize the molecular conformation and orientation to other spider silks or silks that belong to other animal species. This would help us to understand the relationship between the structure and the mechanical properties of silk.

The authors are grateful to Dr. Tetsuo Asakura (Dept. of Biotechnology, Tokyo University of Agriculture and Technology, Tokyo, Japan) for providing us with the *S. c. ricini* cocoon samples and the fibroin primary structure. They also express their gratitude to Serge Groleau and François Lapointe for valuable technical support.

Funding for the Raman spectrometer was obtained through a grant from the Canadian Foundation for Innovation. This work was also supported by the Natural Sciences and Engineering Research Council (NSERC) of Canada and the Fonds Québécois de Recherche sur la Nature et les Technologies (FQRNT). M.-E.R. is indebted to NSERC, FQRNT, and Fondation de l'Université Laval for the award of graduate scholarships.

REFERENCES

1. Denny, M. W. 1980. Silks: their properties and functions. *In* The Mechanical Properties of Biological Materials. Society for Experimental Biology, editors. Cambridge University Press, Cambridge, UK. 246–272.

2. Craig, C. L. 1997. Evolution of arthropod silks. *Annu. Rev. Entomol.* 42: 231–267.
3. Gosline, J. M., M. E. DeMont, and M. W. Denny. 1986. The structure and properties of spider silk. *Endeavour.* 10:37–43.
4. Termonia, Y. 1994. Molecular modeling of spider silk elasticity. *Macromolecules.* 27:7378–7381.
5. Miller, L. D., S. Putthanarat, R. K. Eby, and W. W. Adams. 1999. Investigation of the nanofibrillar morphology in silk fibers by small angle X-ray scattering and atomic force microscopy. *Int. J. Biol. Macromol.* 24:159–165.
6. Putthanarat, S., N. Stribeck, S. A. Fossey, R. K. Eby, and W. W. Adams. 2000. Investigation of the nanofibrils in silk fibers. *Polym.* 41: 7735–7747.
7. Riekel, C., and F. Vollrath. 2001. Spider silk fibre extrusion: combined wide- and small-angle X-ray microdiffraction experiments. *Int. J. Biol. Macromol.* 29:203–210.
8. Oroudjev, E., J. Soares, S. Arcidiacono, J. B. Thompson, S. A. Fossey, and H. G. Hansma. 2002. Segmented nanofibers of spider dragline silk: atomic force microscopy and single-molecule force spectroscopy. *Proc. Natl. Acad. Sci. USA.* 99:6460–6465.
9. Sapede, D., T. Seydel, V. T. Forsyth, M. M. Koza, R. Schweins, F. Vollrath, and C. Riekel. 2005. Nanofibrillar structure and molecular mobility in spider dragline silk. *Macromolecules.* 38:8447–8453.
10. Frische, S., A. B. Maunsbach, and F. Vollrath. 1998. Elongate cavities and skin-core structure in *Nephila* spider silk observed by electron microscopy. *J. Microsc.* 189:64–70.
11. Sponner, A., E. Unger, F. Grosse, and K. Weisshart. 2005. Differential polymerization of the two main protein components of dragline silk during fibre spinning. *Nat. Mater.* 4:772–775.
12. Hernandez Cruz, D., M.-E. Rousseau, M. M. West, M. Pézolet, and A. P. Hitchcock. 2006. Quantitative mapping of the orientation of fibroin β-sheets in *B. mori* cocoon fibers by scanning transmission X-ray microscopy. *Biomacromolecules.* 7:2247–2257.
13. Mita, K., S. Ichimura, and T. C. James. 1994. Highly repetitive structure and its organization of the silk fibroin gene. *J. Mol. Evol.* 38:583–592.
14. Zhou, C.-Z., F. Confalonieri, N. Medina, Y. Zivanovic, C. Esnault, T. Yang, M. Jacquet, M. Duguet, R. Perasso, and Z.-G. Li. 2000. Fine organization of *Bombyx mori* fibroin heavy chain. *Nucleic Acids Res.* 28:2413–2419.
15. Xu, M., and R. V. Lewis. 1990. Structure of a protein superfiber: spider dragline silk. *Proc. Natl. Acad. Sci. USA.* 87:7120–7124.
16. Hinnan, M. B., and R. V. Lewis. 1992. Isolation of a clone encoding a second dragline silk fibroin: *Nephila clavipes* dragline silk is a two-protein fiber. *J. Biol. Chem.* 267:19320–19324.
17. Brooks, A. E., H. B. Steinkraus, S. R. Nelson, and R. V. Lewis. 2005. An investigation of the divergence of Major Ampullate silk fibers from *Nephila clavipes* and *Argiope aurantia*. *Biomacromolecules.* 6: 3095–3099.
18. Sponner, A., B. Schlott, F. Vollrath, E. Unger, F. Grosse, and K. Weisshart. 2005. Characterization of the protein components of *Nephila clavipes* dragline silk. *Biochemistry.* 44:4727–4736.
19. Marsh, R. E., R. B. Corey, and L. Pauling. 1955. An investigation of the structure of silk fibroin. *Biochim. Biophys. Acta.* 16:1–33.
20. Lotz, B., and F. Colonna Cesari. 1979. Chemical structure and the crystalline structures of *Bombyx mori* silk fibroin. *Biochimie.* 61:205–214.
21. Simmons, A., E. Ray, and L. W. Jelinski. 1994. Solid-State ^{13}C NMR of *Nephila clavipes* dragline silk establishes structure and identity of crystalline regions. *Macromolecules.* 27:5235–5237.
22. Kümmerlen, J., J. D. van Beek, F. Vollrath, and B. H. Meier. 1996. Local structure in spider dragline silk investigated by two-dimensional spin-diffusion nuclear magnetic resonance. *Macromolecules.* 29:2920–2928.
23. Asakura, T., T. Ito, M. Okudaira, and T. Kameda. 1999. Structure of alanine and glycine residues of *Samia cynthia ricini* silk fibers studied with solid-state ^{15}N and ^{13}C NMR. *Macromolecules.* 32:4940–4946.
24. van Beek, J. D., L. Beaulieu, M. Demura, T. Asakura, and B. H. Meier. 2000. Solid-state NMR determination of the secondary structure of *Samia cynthia ricini*. *Nat. Mater.* 405:1077–1079.
25. Asakura, T., J. M. Yao, T. Yamane, K. Umemura, and A. S. Ulrich. 2002. Heterogeneous structure of silk fibers from *Bombyx mori* resolved by ^{13}C solid state NMR spectroscopy. *J. Am. Chem. Soc.* 124:8794–8795.
26. Asakura, T., R. Sugino, T. Okuma, and Y. Nakazawa. 2002. The role of irregular unit, GAAS, on the secondary structure of *Bombyx mori* silk fibroin studied with ^{13}C CP/MAS NMR and wide-angle X-ray scattering. *Protein Sci.* 11:1873–1877.
27. Zhou, C.-Z., F. Confalonieri, M. Jacquet, R. Perasso, Z.-G. Li, and J. Janin. 2001. Silk fibroin: structural implications of a remarkable amino acid sequence. *Proteins.* 44:119–122.
28. Hayashi, C. Y., and R. V. Lewis. 1998. Evidence from flagelliform silk cDNA for the structural basis of elasticity and modular nature of spider silks. *J. Biol. Mol.* 275:773–784.
29. Simmons, A. H., C. A. Michal, and L. W. Jelinski. 1996. Molecular orientation and two-component nature of the crystalline fraction of spider dragline silk. *Science.* 271:84–87.
30. Thiel, B. L., K. B. Guess, and C. Viney. 1997. Non-periodic lattice crystals in the hierarchical microstructure of spider (*major ampullate*) silk. *Biopolymers.* 41:703–719.
31. Grubb, D. T., and L. W. Jelinski. 1997. Fiber morphology of spider silk: the effects of tensile deformation. *Macromolecules.* 30:2860–2867.
32. Fossey, S. A., and S. Tripathy. 1999. Atomistic modeling of interphases in spider silk fibers. *Int. J. Biol. Macromol.* 24:119–125.
33. Valluzzi, R., S. Szela, P. Avtges, D. Kirschner, and D. Kaplan. 1999. Methionine redox-controlled crystallization of biosynthetic silk spidroin. *J. Phys. Chem. B.* 103:11382–11392.
34. van Beek, J. D., S. Hess, F. Vollrath, and B. H. Meier. 2002. The molecular structure of spider dragline silk: folding and orientation of the protein backbone. *Proc. Natl. Acad. Sci. USA.* 99:10266–10271.
35. Eles, P. T., and C. A. Michal. 2004. A DECODER NMR study of backbone orientation in *Nephila clavipes* dragline silk under varying strain and draw rate. *Biomacromolecules.* 5:661–665.
36. Holland, G. P., R. V. Lewis, and J. L. Yarger. 2004. WISE NMR characterization of nanoscale heterogeneity and mobility in super-contracted *Nephila clavipes* spider dragline silk. *J. Am. Chem. Soc.* 126:5867–5872.
37. Asakura, T., K. Ohgo, K. Komatsu, M. Kanenari, and K. Okuyama. 2005. Refinement of repeated β-turn structure for silk I conformation of *Bombyx mori* fibroin using ^{13}C solid-state NMR and X-ray diffraction method. *Macromolecules.* 38:7397–7403.
38. Riekel, C., C. Bräden, C. L. Craig, C. Ferrero, F. Heidelbach, and M. Müller. 1999. Aspects of X-ray diffraction on single spider fibers. *Int. J. Biol. Macromol.* 24:179–186.
39. Rousseau, M.-E., T. Lefevre, L. Beaulieu, T. Asakura, and M. Pezolet. 2004. Study of protein conformation and orientation in silkworm and spider silk fibers using Raman microspectroscopy. *Biomacromolecules.* 5:2247–2257.
40. Lefevre, T., M.-E. Rousseau, and M. Pézolet. 2006. Orientation-insensitive spectra for Raman microspectroscopy. *Appl. Spectrosc.* 60: 841–846.
41. Lagugné-Labarthet, F., J.-L. Bruneel, T. Buffeteau, C. Sourisseau, M. R. Huber, S. J. Zilker, and T. Bieringer. 2000. Photoinduced orientations of a azobenzene in two distinct holographic diffraction gratings as studied by polarized Raman confocal microspectroscopy. *Phys. Chem. Chem. Phys.* 2:5154–5167.
42. Lagugné-Labarthet, F., T. Buffeteau, and C. Sourisseau. 1998. Molecular orientations in azopolymer holographic diffraction gratings as studied by Raman confocal microspectroscopy. *J. Phys. Chem. B.* 102:5754–5765.
43. Pajcini, V., X. G. Chen, R. W. Bormett, S. J. Geib, P. Li, S. A. Asher, and E. G. Lidiak. 1996. Glycylglycine π-π^* and charge transfer transition moment orientations: near-resonance Raman single-crystal measurements. *J. Am. Chem. Soc.* 118:9716–9726.

44. Tsuboi, M., Y. Kubo, K. Akahane, J. M. Benevides, and G. J. Thomas. 2006. Determination of the amide I Raman tensor for the antiparallel β-sheet: application to silkworm and spider silks. *J. Raman Spectrosc.* 37:204–247.

45. Rousseau, M.-E., L. Beaulieu, T. Lefevre, J. Paradis, T. Asakura, and M. Pézolet. 2006. Characterization by Raman spectroscopy of the strain-induced conformational transition in fibroin fibers from the silkworm *Samia cynthia ricini*. *Biomacromolecules.* 7:2512–2521.

46. Berne, B. J., P. Pechukas, and G. D. Harp. 1968. Molecular reorientation in liquids and gases. *J. Chem. Phys.* 49:3125–3129.

47. Bower, D. I. 1981. Orientation distribution functions for uniaxially oriented polymers. *J. Polym. Sci. [B].* 19:93–107.

48. Frisk, S., R. M. Ikeda, D. B. Chase, and J. F. Rabolt. 2003. Rotational invariants for polarized Raman spectroscopy. *Appl. Spectrosc.* 57: 1053–1057.

49. Moore, W. H., and S. Krimm. 1976. Vibrational analysis of peptides, polypeptides, and proteins. II. β-Poly(L-alanine) and β-poly(L-alanylglycine). *Biopolymers.* 15:2465–2483.

50. Krimm, S., and J. Bandekar. 1986. Vibrational spectroscopy and conformation of peptides, polypeptides, and proteins. *Adv. Protein Chem.* 38:181–364.

51. Takahashi, Y., M. Gehoh, and K. Yuzuriha. 1999. Structure refinement and diffuse streak scattering of silk (*Bombyx mori*). *Int. J. Biol. Macromol.* 24:127–138.

52. Witter, R., U. Sternberg, and A. S. Ulrich. 2005. NMR chemical shift powder pattern recoupling at high spinning speed and theoretical tensor evaluation applied to silk fibroin. *J. Am. Chem. Soc.* 128:2236–2243.

53. Hsu, S. L., W. H. Moore, and S. Krimm. 1976. Vibrational spectrum of unordered polypeptide chain: Raman study of feather keratin. *Biopolymers.* 15:1513–1528.

54. Maiti, N. C., M. M. Apetri, Z. M. G., P. R. Carey, and V. E. Anderson. 2004. Raman spectroscopic characterization of secondary structure in natively unfolded proteins: α-synuclein. *J. Am. Chem. Soc.* 126:2400–2408.

55. Vass, E., M. Hollosi, F. Besson, and R. Buchet. 2003. Vibrational spectroscopic detection of β- and γ-turns in synthetic and natural peptides and proteins. *Chem. Rev.* 103:1917–1954.

56. Krimm, S., and J. Bandekar. 1980. Vibrational analysis of peptides, polypeptides, and proteins. 5. Normal vibrations of β-turns. *Biopolymers.* 19:1–29.

57. Gatesy, J., C. Hayashi, D. Motriuk, J. Woods, and R. Lewis. 2001. Extreme diversity, conservation, and convergence of spider silk fibroin sequences. *Science.* 291:2603–2605.

58. Rengasamy, R. S., M. Jassal, and C. Rameshkumar. 2005. Studies on structure and properties of *Nephila* spider silk dragline. *AUTEX Res. J.* 5:30–39.

59. Warner, S. B., K. Beckham, B. Pourdeyhimi, and D. Grubb. 1995. Development of low cost moderately high strength, tough fibers for industrial applications. *Nat. Textile Center Res. Briefs.* G95–8:4–5.

60. Inoue, S.-I., N. Kawasaki, J. Magoshi, and Y. Amemiya. 2002. 2003. Synchrotron X-ray diffraction of single silk fiber spun by younger instar silkworm larvae. *Photon Factory Activity Report.* 20:188.

61. Lucas, F., J. T. B. Shaw, and S. G. Smith. 1956. Amino-acid sequence in a fraction of *Bombyx* silk fibroin. *Nature.* 178:861.

62. Izuka, E. 1965. Degree of crystallinity and modulus relationships of silk thread from cocoons of *Bombyx mori* L. and other moths. *Biorheology.* 3:1–8.

63. Hutchinson, E. G., and J. M. Thornton. 1994. A revised set of potentials for β-turn formation in proteins. *Protein Sci.* 3:2207–2216.

64. Liu, Y., Z. Shao, and F. Vollrath. 2005. Relationships between supercontraction and mechanical properties of spider silk. *Nat. Mater.* 4:901–905.